

On the 2D behavior of 3D MHD with a strong guiding field

Alexandros Alexakis

*Laboratoire de Physique Statistique de l'Ecole Normale Supérieure,
UMR CNRS 8550, 24 Rue Lhomond, 75006 Paris Cedex 05, France.*

(Dated: February 18, 2022)

The Magneto-hydrodynamic (MHD) equations in the presence of a guiding magnetic field are investigated by means of direct numerical simulations. The basis of the investigation consists of 9 runs forced at the small scales. The results demonstrate that for a large enough uniform magnetic field the large scale flow behaves as a two dimensional (non-MHD) fluid exhibiting an inverse cascade of energy in the direction perpendicular to the magnetic field, while the small scales behave like a three dimensional MHD-fluid cascading the energy forwards. The amplitude of the inverse cascade is sensitive to the magnetic field amplitude, the domain size, the forcing mechanism, and the forcing scale. All these dependencies are demonstrated by the varying parameters of simulations. Furthermore, in the case that the system is forced anisotropically in the small parallel scales an inverse cascade in the parallel direction is observed that is feeding the 2D modes $k_{\parallel} = 0$.

I. INTRODUCTION

The existence of magnetic fields is known in many astrophysical objects, such as the interstellar medium, galaxies, accretion disks, star and planet interiors and the solar wind [1]. In most of these systems, the magnetic fields are strong enough to play a significant dynamical role. The kinetic and magnetic Reynolds numbers involved in these astrophysical bodies are large enough so that the flows exhibit a turbulent behavior with a large continuous range of excited scales, from the largest where energy is injected, toward the finest where energy is dissipated. In many cases, strong large-scale magnetic fields are present that induce dynamic anisotropy in the small scales. Direct numerical simulations that examine in detail both large and small scale turbulent processes in astrophysical plasmas are very difficult to achieve, and only modest scale separation can be reached even with today's super-computers. One way around this difficulty is to model the effect of the large scale field by a uniform magnetic field B_0 , and thus study the small scales separately.

In the presence of a strong uniform magnetic field the evolution of the turbulent fluctuating fields can be treated within the framework of weak turbulence theory (WTT). In this approach the nonlinearities are treated perturbatively, resulting in a slowly varying amplitude of the linear wave modes that in this case are the Alfvén waves supported by the uniform magnetic field [2, 3]. However, the limit $B_0 \rightarrow \infty$ is non-trivial because different limiting procedures can lead to different results. Thus in order for the results of weak turbulence theory [2] to hold a domain of size L (in direction of the field) sufficiently large needs to be considered, so that modes with small wave numbers in the direction of the field that satisfy the “quasi-resonance” conditions are present. In particular WTT is valid when the following condition is met:

$$\frac{1}{\sqrt{k_{\parallel} L_{\parallel}}} \ll \frac{u_k k_{\perp}}{B_0 k_{\parallel}} \ll 1 \quad (1)$$

(see [4]) where $|u_k|$ is the amplitude of the velocity field with wavenumbers $\sim \mathbf{k}$ (with k_{\parallel} and k_{\perp} the parallel and perpendicular projection of \mathbf{k} to the magnetic field respectively). L_{\parallel} is the domain size in the direction of the field. The inequality on the right implies sufficiently weak nonlinearity while the inequality on the left is needed for the presence of quasi resonances. In this case WTT predicts that the energy spectrum is proportional to k_{\perp}^{-2} . On the other hand if

$$\frac{|u_k| k_{\perp}}{B_0 k_{\parallel}} \ll \frac{1}{k_{\perp} L_{\perp}} \frac{1}{\sqrt{k_{\parallel} L_{\parallel}}} \quad (2)$$

the system becomes “slaved” to the 2D modes $k_{\parallel} = 0$ that evolve independently [4]. Thus if the limit $B_0 \rightarrow \infty$ is taken keeping the domain size L fixed the system becomes two dimensional [4, 5]. Note that the two conditions (1),(2) allow the existence of an intermediate regime.

Here the large B_0 limit is explored further by means of numerical simulations. Numerically, magneto-hydrodynamic (MHD) turbulence has been investigated by various groups in the last decade [6–10]. The results of WTT were first demonstrated in [11, 12] while the transition to two dimensional dynamics has been investigated more recently in [13]. In all these investigations the flow was forced in the largest scale of the system. In this work the case where the system is forced in the small scales is explored and the possible development of an inverse cascade is examined.

An inverse energy cascade is known to exist in two-dimensional (2D) hydrodynamic turbulence [14–16], as a consequence of the conservation of vorticity. It results in a $k^{-5/3}$ spectrum for the large scales and a k^{-3} spectrum for the small scales. Strongly rotating flows [17–21] or flows in thin boxes [22] have been shown to have a dual cascade of energy with the large scale flow behaving like 2D with an inverse cascade while the small scales being three dimensional with a direct cascade. However, 2D MHD turbulence does not conserve the vorticity and energy is cascading to small scales. On the contrary the square of the vector potential is cascading to larger

scales [23, 24]. For the system under investigation we cannot a priori predict if the flow under the influence of a strong magnetic field will act as a 2D-*hydrodynamic* flow by suppressing all magnetic fluctuations and thus have an inverse cascade; or if magnetic fluctuations persist and the system will act as a 2D-MHD flow and thus not exhibit an inverse cascade of energy. It is noted that a strong magnetic field is used very often to make flows of liquid metals behaving like two dimensional flows in experiments where an inverse cascade has been observed [25, 26]. These flows however have very small magnetic Reynolds numbers and magnetic fluctuations are strongly suppressed.

II. FORMULATION AND NUMERICAL SIMULATIONS

We consider a flow of a conducting fluid inside a triple-periodic box of size $2\pi L$ in the presence of a strong guiding magnetic field B_0 in the $\hat{\mathbf{z}}$ direction. The system is forced by a mechanical force \mathbf{f} and an electro-motive force \mathcal{E} . The non-dimensional MHD equations then read:

$$\begin{aligned}\partial_t \mathbf{u} + \mathbf{u} \cdot \nabla \mathbf{u} &= V_A \partial_z \mathbf{b} + \mathbf{b} \cdot \nabla \mathbf{b} - \nabla P + G_\kappa^{-\frac{1}{2}} \nabla^2 \mathbf{u} + \mathbf{F} \\ \partial_t \mathbf{b} + \mathbf{u} \cdot \nabla \mathbf{b} &= V_A \partial_z \mathbf{u} + \mathbf{b} \cdot \nabla \mathbf{u} + G_M^{-\frac{1}{2}} \nabla^2 \mathbf{b} + M \nabla \times \mathbf{E},\end{aligned}$$

where \mathbf{u} is the velocity field and \mathbf{b} is the magnetic field. Both fields are assumed to be solenoidal $\nabla \cdot \mathbf{u} = \nabla \cdot \mathbf{b} = 0$. $\mathbf{F} = \mathbf{f}/\|\mathbf{f}\|$ is the external mechanical force normalized to unit amplitude (where $\|\cdot\|$ stands for the L_2 norm). \mathbf{E} is the external electro-motive force normalized so that its curl has unit amplitude $\mathbf{E} = \mathcal{E}/\|\nabla \times \mathcal{E}\|L$. The equations have been non-dimensionalized using the box size L and the forcing amplitude $\|\mathbf{f}\|$. With this choice four non-dimensional parameters appear. G_κ is the kinetic Grasshof number $G_\kappa \equiv \|\mathbf{f}\|L^3/\nu^2$, where ν is the viscosity. G_M is the magnetic Grasshof number $G_M \equiv \|\mathbf{f}\|L^3/\eta^2$, where η is the magnetic diffusivity. In all the runs performed in this work $G_\kappa = G_M$. The amplitude of the external magnetic field relative to the forcing is controlled by the parameter $V_A \equiv B_0/\sqrt{\|\mathbf{f}\|L}$. Finally $M \equiv \|\nabla \times \mathcal{E}\|/\|\mathbf{f}\|$ expresses the ratio of the electro-motive to the mechanical forcing.

A possible alternative to this non-dimensionalization choice would be to use the kinetic and magnetic Reynolds numbers, typically defined as $Re \equiv \|\mathbf{u}\|L/\nu$ and $Rm \equiv \|\mathbf{u}\|L/\eta$ respectively. For our problem at hand however where an inverse cascade is present it is not an attractive choice because the amplitude of the velocity is changing with time throughout the duration of the computation rendering Re a function of time.

Both forcing mechanisms used in the numerical simulations consisted of a sum of Fourier modes with wavenumbers inside a spherical shell $|\mathbf{k}| = k_f$. The phases of the modes were changed randomly every time interval $\tau \sim \sqrt{L}/\|\mathbf{f}\|$. The forcing is isotropic in all runs except the last two that we discuss in section III E. There was no

RUNS	$G_\kappa^{-\frac{1}{2}}/10^3$	V_A	$k_f L$	M_0	Isotropy
R1	5.0	5.0	8-10	0.0	I
R2	2.5	2.0	8-10	0.0	I
R3	2.5	10.0	8-10	0.0	I
R4	10.0	5.0	4-5	0.0	I
R5	2.5	5.0	16-20	0.0	I
R6	3.3	5.0	8-10	0.4	I
R7	2.5	5.0	8-10	0.6	I
R8	2.5	5.0	8-10	0.0	$\mathbf{F}(\mathbf{k}_\parallel, \mathbf{0}) = \mathbf{0}$
R9	16.0	5.0	8-10	0.0	$\mathbf{F}(\mathbf{0}, \mathbf{k}_\perp) = \mathbf{0}$

TABLE I. Table with the parameters of all runs. “I” in the last column stands for isotropic forcing. With boldface are marked the parameters that are varied with respect to R1.

averaged helicity or cross-helicity injected by the forcing by choosing: $\langle \mathbf{F} \cdot \nabla \times \mathbf{F} \rangle = 0$ and $\langle \mathbf{F} \cdot \nabla \times \mathbf{E} \rangle = 0$. Since we are interested in the presence of an inverse cascade we are forcing relatively large wave numbers.

The MHD equations were solved using a standard pseudo-spectral method and a third order in time Runge-Kuta [27, 28]. The resolution used in all the runs was 512^3 grid points. In the 9 different runs that were performed the amplitude of the external magnetic field, and the way the system is forced was varied. The table II gives all the parameters of the runs.

The choice of G_κ in most runs is rather conservative because it is not known beforehand what effect on the resolution requirements a change in each of the parameters has. In any case, in all runs a well resolved spectrum was observed. The last run (R9) has a large value of G_κ because in this case for similar forcing amplitude with the other runs the flow is less efficient in absorbing energy because the $k_\parallel = 0$ modes are not forced. In this run also the time scale of the forcing was set to $\tau \sim (B_0 k_f)^{-1}$ to be closer in resonance with the forced Alfvén-modes and to improve this absorption efficiency.

The diagnostics used are based on energy spectra and energy fluxes that are now defined. If $\hat{\mathbf{u}}_{\mathbf{k}}$ and $\hat{\mathbf{b}}_{\mathbf{k}}$ are the Fourier modes of the velocity and magnetic field of wavenumber \mathbf{k} then the two dimensional energy spectra $E_u(k_\perp, k_\parallel)$ and $E_b(k_\perp, k_\parallel)$ are defined as

$$E_u(k_\perp, k_\parallel) = \frac{1}{2} \sum |\hat{\mathbf{u}}_{\mathbf{k}}|^2, \quad E_b(k_\perp, k_\parallel) = \frac{1}{2} \sum |\hat{\mathbf{b}}_{\mathbf{k}}|^2$$

where the sum is restricted in the wavenumbers $k_\parallel \leq |k_z| < k_\parallel + 1$ and $k_\perp \leq \sqrt{k_x^2 + k_y^2} < k_\perp + 1$. The averaged energy spectra in the parallel direction are then defined as

$$\bar{E}_u(k_\perp) = \sum_{k_\parallel} E_u(k_\perp, k_\parallel), \quad \bar{E}_b(k_\perp) = \sum_{k_\parallel} E_b(k_\perp, k_\parallel).$$

The total kinetic energy E_K and magnetic energy E_M are then given by

$$E_K = \sum_{k_\perp} \bar{E}_u(k_\perp), \quad E_M = \sum_{k_\perp} \bar{E}_b(k_\perp).$$

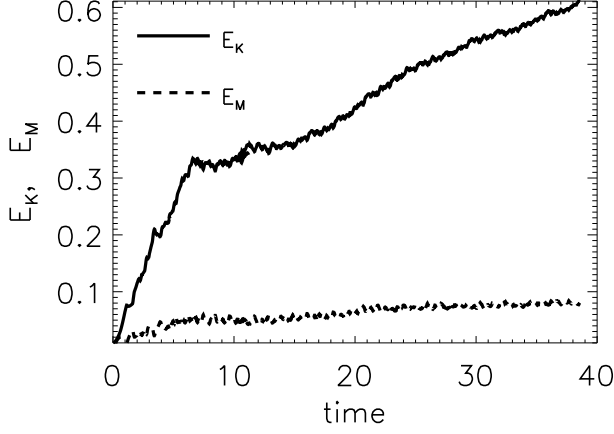


FIG. 1. Time evolution of the kinetic energy E_K (solid line) and the magnetic energy E_M (dashed line) for run R1.

Since the development of a direct or an inverse cascade is expected to be anisotropic we need to define the flux of energy through an arbitrary surface in Fourier space. If \mathbf{u}_D and \mathbf{b}_D stand for the projection of the two fields \mathbf{u}, \mathbf{b} to the flows whose Fourier transform contain modes only inside the Fourier domain “D”, the energy flux through this domain is given by

$$\Pi_D = \int [\mathbf{u}_D \cdot \nabla \mathbf{u} - \mathbf{u}_D \cdot \nabla \mathbf{b} + \mathbf{b}_D \cdot \nabla \mathbf{u} - \mathbf{b}_D \cdot \nabla \mathbf{b}] dV.$$

See [29] for more details. In this work we will consider the flux through cylinders and planes. By $\Pi_\perp(k_\perp)$ we will refer to the flux of energy through a cylinder of radius $\sqrt{k_x^2 + k_y^2} = k_\perp$ and by $\Pi_\parallel(k_\parallel)$ we will refer to the flux of energy through the planes $|k_z| = k_\parallel$. Positive flux implies cascade of energy to the small scales while a negative flux implies cascade to the large scales.

III. RESULTS

A. A pilot run

The first run in table I serves as a basic run to which all other runs are compared. For this reason this run is examined in more detail. Figure 1 shows the evolution of the kinetic and magnetic energy as a function of time. As can be seen the magnetic energy grows and saturates very fast at a relatively small amplitude. The kinetic energy on the other hand, after an initial fast growth transitions to a slower increasing phase. Up until the end of the numerical simulation this slow growth persists. The reason for this growth is the inverse cascade of the kinetic energy that accumulates energy in the large scales.

This inverse cascade is demonstrated more clearly in figure 2. This figure shows the parallel and perpendicular energy flux normalized by the total energy injection rate. The perpendicular energy flux is positive for wavenumbers larger than the forcing wavenumber (direct cascade)

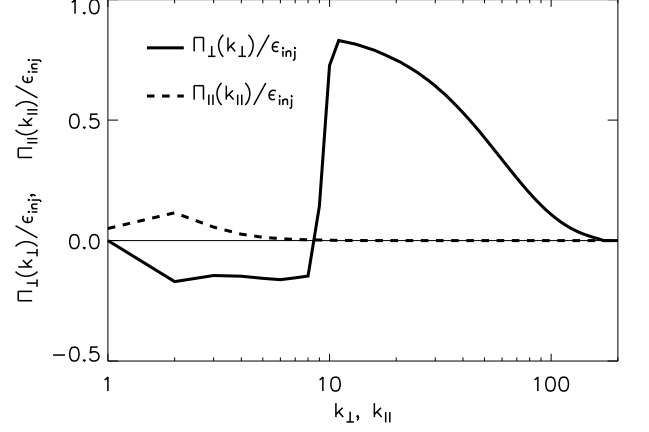


FIG. 2. The energy flux for run R1 in the perpendicular direction (solid line) and parallel direction (dashed line).

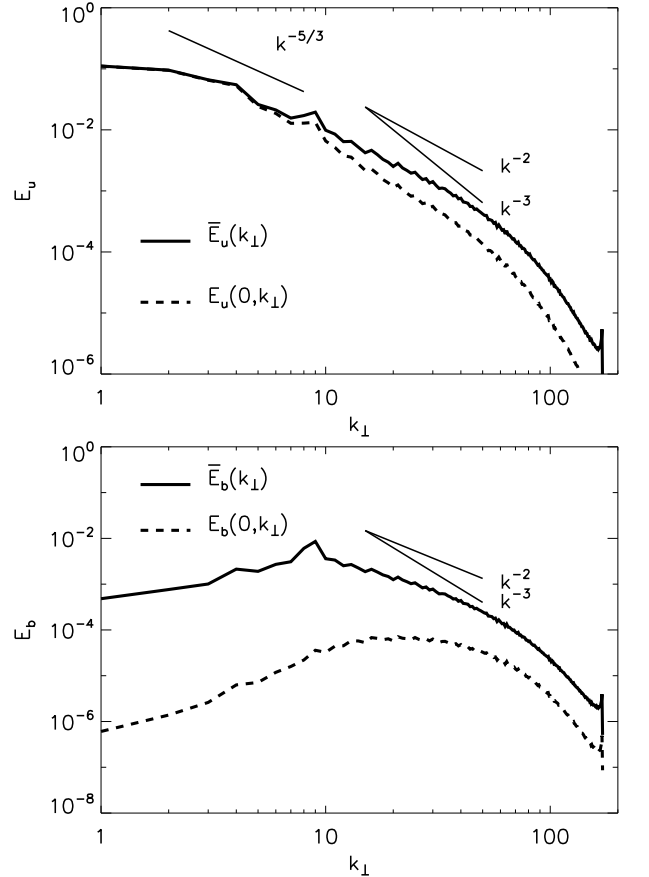


FIG. 3. Kinetic (top panel) and magnetic (bottom panel) energy spectra of run R1. The solid lines correspond to the averaged spectra $\bar{E}_u(k_\perp), \bar{E}_b(k_\perp)$ while the dashed lines indicate the zeroth component ($k_\parallel = 0$) of the two dimensional energy spectra $E_u(0, k_\perp)$ and $E_b(0, k_\perp)$. The straight lines show for reference the power law spectra $k^{-5/3}, k^{-2}, k^{-3}$.

while for smaller wave numbers a negative constant energy flux (inverse cascade) can be seen. On the other hand the parallel energy flux, shown by the dashed line, is small and always positive (*ie* direct).

The presence of an inverse cascade can also be indicated by looking at the energy spectra at late times. The top panel of figure 3 shows the kinetic energy spectrum \bar{E}_u of run R1 averaged over several outputs close to the end of the simulation. It can be clearly seen that most of the energy is concentrated in the large scales. The dashed line in this panel shows $E_u(0, k_\perp)$. At large scales this line is identical to the \bar{E}_u spectrum thus the energy in these scales is mostly contained in the 2D-modes $k_\parallel = 0$. This means that the flow in the large scales is almost 2D. (Here the flow is referred to as 2D in the sense that u has no dependence on the z -direction and not that the u_z component is absent.) On the other hand at the small scales $E_u(0, k_\perp)$ is significantly smaller than \bar{E}_u thus the 2D-modes contain only a small fraction of the energy and therefor the flow is three-dimensional.

The bottom panel of fig 3 compares the magnetic energy spectra $E_b(0, k_\perp)$ and \bar{E}_b . Unlike the velocity field the magnetic field remains strongly three-dimensional for all scales since $E_b(0, k_\perp) \ll \bar{E}_b$. The amplitude of the magnetic energy is much smaller than that of the kinetic energy in the large scales but of the same order in the small scales. This is essential for the presence of the 2D-inverse cascade. If the magnetic field fluctuations were strong enough in the large scales the flow would behave as a 2D-MHD flow with a direct cascade.

The $k^{-5/3}$ scaling prediction for the 2D inverse cascade, the k^{-3} for the direct 2D cascade and the k^{-2} prediction of WTT are shown as a reference. The observed spectra are compatible with $k^{-5/3}$ in the large scales and k^{-2} in the small scales however the inertial ranges in the examined flow are too small to be conclusive.

B. Guiding magnetic field strength

As a next step the dependence of the inverse cascade, observed in R1, on the amplitude of the uniform magnetic field is examined. Runs R2 and R3 have all parameters similar to run R1 but different value of the magnetic field amplitude. The flux of energy in both directions for the runs R1, R2 and R3 are compared in figure 4. As expected the amplitude of the uniform magnetic field has a drastic effect on the energy flux. The top panel of this figure shows $\Pi_\perp(k_\perp)$. R2 (dashed line) that has smaller value of V_A than run R1 (solid line) has no inverse cascade and a stronger direct cascade. R3 (dashed-dot line) that has larger value of V_A has on the contrary a stronger inverse cascade and a weaker forward cascade. The bottom panel of figure 4 shows the energy flux in the parallel direction. As the magnetic field is increased the flux to large k_z is decreased. This is expected since in the $V_A = \infty$ limit there is cascade only in perpendicular direction.

The spectra for these runs are compared in figure 5.

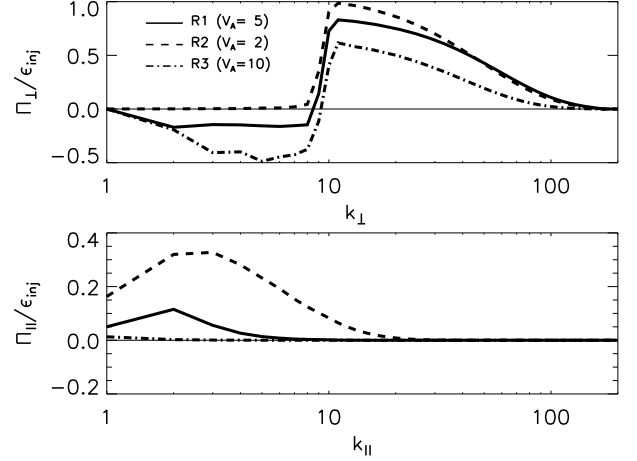


FIG. 4. Top panel: The energy flux in the perpendicular direction for R1 ($V_A = 5$, solid line), R2 ($V_A = 2$, dashed line), R3 ($V_A = 10$, dashed-dot line). Bottom panel: The energy flux in the parallel direction for the same runs.

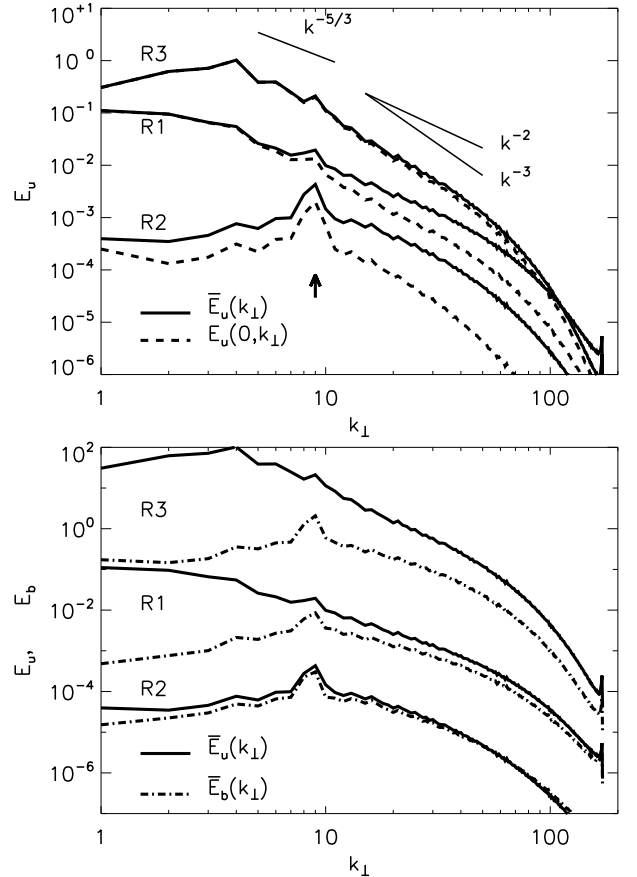


FIG. 5. Top panel: The kinetic energy spectra of $\bar{E}_u(k_\perp)$ (solid line), and $E_u(0, k_\perp)$ (dashed line) for R3, $V_A = 10$ (top lines), R1, $V_A = 5$ (middle lines), R2, $V_A = 2$ (bottom lines). Bottom panel: The kinetic energy spectra $\bar{E}_u(k_\perp)$ (solid line), compared to the magnetic energy spectra $\bar{E}_b(k_\perp)$ (dashed line) of the same runs and with the same order. The spectra have been shifted for reasons of clarity.

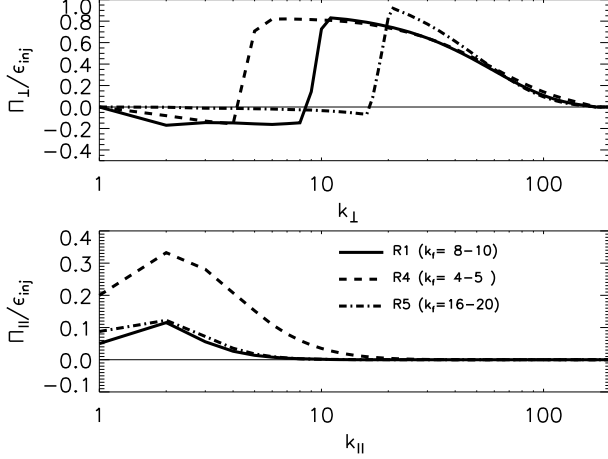


FIG. 6. Top panel: The energy flux in the perpendicular direction for R1 ($8 < k_f \leq 10$, solid line), R4 ($4 < k_k \leq 5$, dashed line), R5 ($16 < k_f \leq 20$, dashed-dot line). Bottom panel: The energy flux in the perpendicular direction for the same runs.

The top panel of this figure shows the kinetic energy spectra $\bar{E}_u(k_{\perp})$ and $E_u(0, k_{\perp})$. The spectra have been shifted for reasons of clarity. In the two runs R1 and R3 that showed an inverse cascade, energy is concentrated in the largest scales. What can also be observed is that as V_A is increased the flow comes closer to a two dimensional flow. For R2 for which $V_A = 2$ and no inverse cascade is observed the flow is far from two dimensional even at the largest scales.

The bottom panel of figure 5 compares the kinetic energy spectra $\bar{E}_u(k_{\perp})$ (solid line) with the magnetic energy spectra $\bar{E}_b(k_{\perp})$ (dashed line). As the uniform magnetic field is increased the magnetic fluctuations are decreased compared to the velocity fluctuations. Note that for R3 the magnetic fluctuations are almost negligible in all scales while for R2 the two fluctuating fields are in equipartition. A possible interpretation of for this behavior is the following. Since in these runs there is no forcing for the magnetic field the magnetic fluctuations can be generated only by the stretching of field lines of the uniform component or by a dynamo mechanism. However since the flow comes close to a 2D flow as V_A is increased neither of these mechanisms is possible. The dynamo mechanism however could depend on the magnetic Reynolds number that for these runs it is relatively small.

C. Forcing scale

The second parameter we examine is the forcing scale $k_f L$. This parameter is important because it controls the number of modes that satisfy the quasi-resonance conditions (1),(2). The energy flux of runs R4 with $4 < k_f \leq 5$ and R5 with $16 < k_f \leq 20$ are compared to the energy flux of R1 with $8 < k_f \leq 10$ in figure 6. The top panel

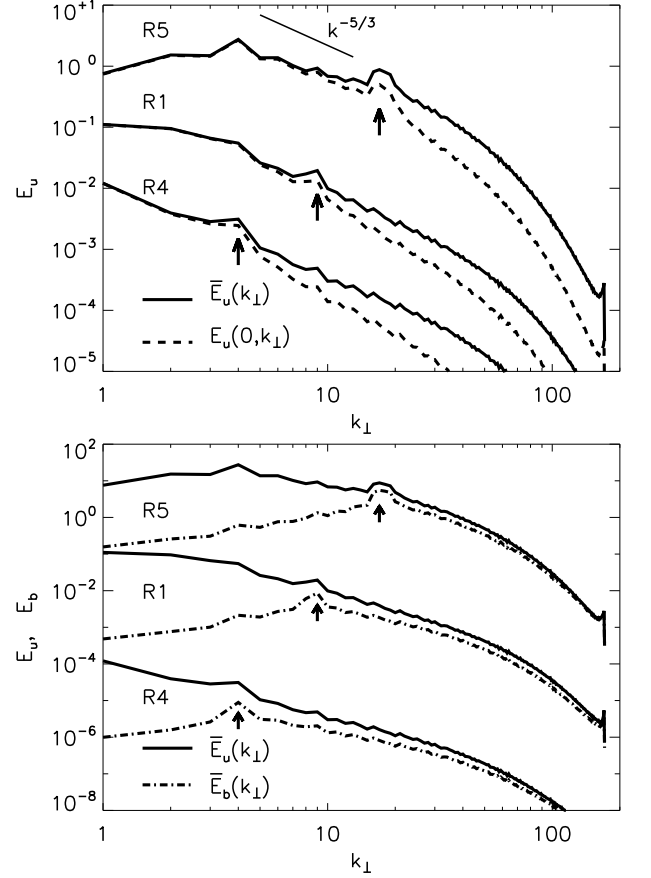


FIG. 7. Top panel: The kinetic energy spectra of $\bar{E}_u(k_{\perp})$ (solid line), and $E_u(0, k_{\perp})$ (dashed line) for R5, (top lines), R1, (middle lines), R4, (bottom lines) Bottom panel: The kinetic energy spectra $\bar{E}_u(k_{\perp})$ (solid line), compared to the magnetic energy spectra $\bar{E}_b(k_{\perp})$ (dashed line) of the same runs and with the same order. The spectra have been shifted for reasons of clarity. The arrows indicate the location of the forcing.

again shows the energy flux in the perpendicular direction while the bottom panel shows the energy flux in the parallel direction.

All flows show an inverse cascade in the perpendicular direction. R4 has an inverse cascade of the same amplitude with R1 while R5 that is forced in smaller scales has a weaker inverse cascade. This is somehow expected since when the forcing is in smaller scales the system is closer in violating condition (2) for 2D behavior. Note also that R4 has a larger flux in the parallel direction.

The spectra for these runs are shown in figure 7. All runs have most of the kinetic energy concentrated in the large scales that behave like 2D-hydrodynamic flows: $\bar{E}_u(k_{\perp}) \simeq E_u(0, k_{\perp})$ (top panel) and $\bar{E}_u(k_{\perp}) \gg \bar{E}_b(k_{\perp})$ (bottom panel). The scales smaller than the forcing scale on the other hand behave like 3D-MHD flows with $\bar{E}_u(k_{\perp}) > E_u(0, k_{\perp})$ and $\bar{E}_u(k_{\perp}) \simeq \bar{E}_b(k_{\perp})$.

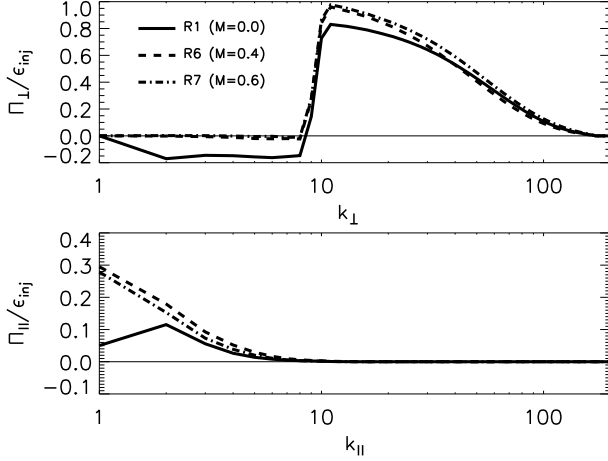


FIG. 8. Top panel: The energy flux in the perpendicular direction for R1 ($M = 0$, solid line), R6 ($M = 0.4$, dashed line), R7 ($M = 0.6$, dashed-dot line). Bottom panel: The energy flux in the perpendicular direction for the same runs.

D. Mechanical and electro-motive forcing

The inverse cascade observed in some of the discussed runs is a property of 2D hydrodynamic turbulence that is not present in 2D-MHD turbulence. The reason it appears in the previous runs is that the amplitude of the magnetic field fluctuations in the large scales remains weak. This effect could possibly be destroyed by a large scale dynamo at larger magnetic Reynolds numbers. Leaving this possibility open the existence of the inverse cascade is investigated when magnetic field fluctuations are amplified by an electro-motive force. This is examined in runs R6 and R7 where both the mechanical and the electro-motive force are present.

Figure 8 shows the energy flux for runs R6 with $M = 0.4$ and R7 with $M = 0.6$ compared with R1 for which $M = 0$. The introduction of the electro-motive force ($M \neq 0$) destroys the inverse cascade in the perpendicular direction (top panel), while little change is observed in the parallel direction (bottom panel). This change indicates that the system transitions from an hydrodynamic 2D state to a forward cascading MHD state.

This is further confirmed by looking at the energy spectra in figure 9. The top panel compares again the kinetic energy spectra $\bar{E}_u(k_{\perp})$ and $E_u(0, k_{\perp})$. The excess of kinetic energy that is present in the large scales for run R1, is absent in runs R6 and R7, verifying further the absence of the inverse cascade in the presence of an electro-motive force. Note that in all runs the large scales are still two-dimensional $\bar{E}_u \simeq E(0, k_{\perp})$ (top panel) but the condition $\bar{E}_u(k_{\perp}) \gg \bar{E}_b(k_{\perp})$ is true only for R1 (bottom panel). This indicates that the absence of the inverse cascades for runs R6 and R7 is not because the flow stops behaving like a 2D flow, but rather because it starts behaving like a 2D-MHD flow.

In 2D-MHD flows however there is an inverse cascade

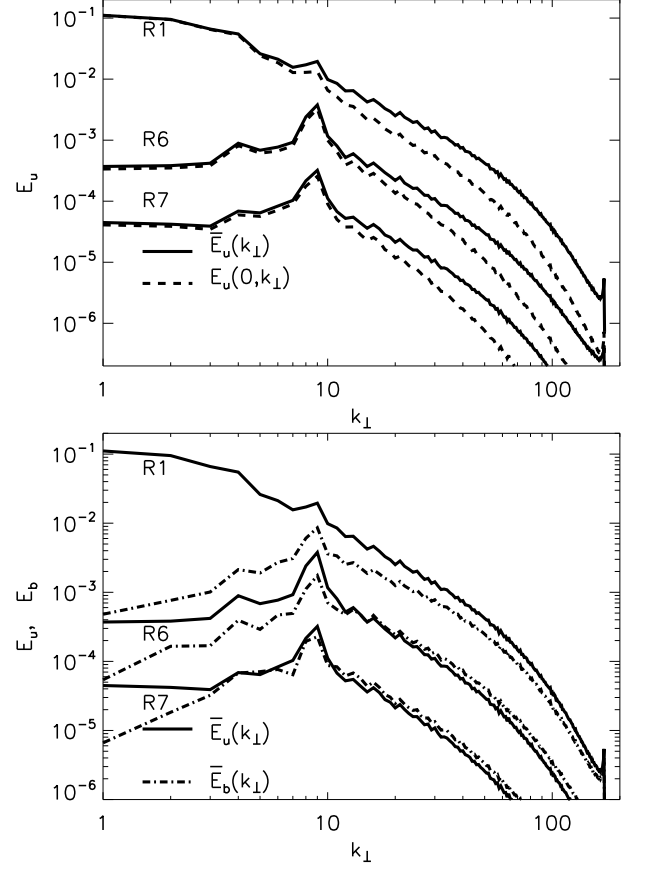


FIG. 9. Top panel: The kinetic energy spectra of $\bar{E}_u(k_{\perp})$ (solid line), and $E_u(0, k_{\perp})$ (dashed line) for R1, $M = 0$ (top lines), R6, $M = 0.4$ (middle lines), R7 $M = 0.6$ (bottom lines). Bottom panel: The kinetic energy spectra $\bar{E}_u(k_{\perp})$ (solid line), compared to the magnetic energy spectra $\bar{E}_b(k_{\perp})$ (dashed line) of the same runs and with the same order. The spectra have been shifted for reasons of clarity.

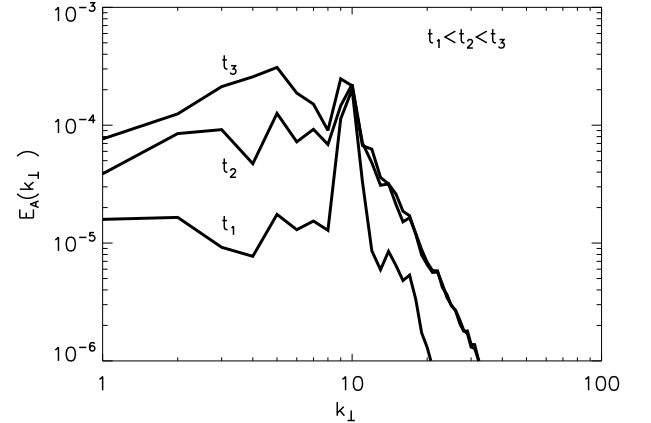


FIG. 10. The vector potential spectrum \bar{E}_A for three different times.

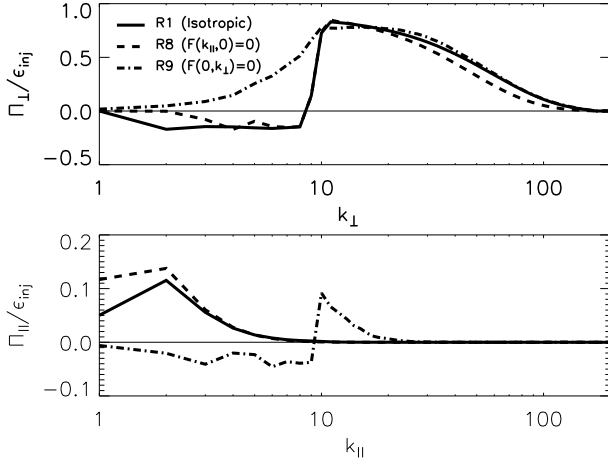


FIG. 11. Top panel: The energy flux in the perpendicular direction for R1 (solid line), R8 (dashed line), R9 (dashed-dot line). Bottom panel: The energy flux in the perpendicular direction for the same runs.

of the square of the vector potential that is a conserved quantity. If the flow in the runs R6 and R7 behave like a 2D MHD flow in the large scales such a cascade should be observed. However a flux for the squared vector potential in three dimensions can not be uniquely defined since it is not a conserved quantity. Nonetheless, we plot the vector potential spectra for three different times from run R7 in figure 10. The vector potential \mathbf{a} is defined so that $\mathbf{b} = \nabla \times \mathbf{a}$ and $\nabla \cdot \mathbf{a} = 0$. Its spectrum is then defined as

$$\bar{E}_A(k_{\perp}) = \frac{1}{2} \sum |\hat{\mathbf{a}}_{\mathbf{k}}|^2 \quad (3)$$

where the sum is restricted in the wavenumbers $k_{\perp} \leq \sqrt{k_x^2 + k_y^2} < k_{\perp} + 1$ and $\hat{\mathbf{a}}_{\mathbf{k}}$ is the Fourier transform of \mathbf{a} . It can be seen that as time progresses the vector potential is increasing in the large scales. It is noted that a quasi-conservation of the square of the vector potential has been observed in [30, 31] for three-dimensional ideal reduced-MHD.

E. Isotropic and anisotropic forcing

The last parameter that we vary is the isotropy of the forcing. Unlike the previously examined runs for which all Fourier modes within a spherical shell are uniformly forced in runs R8 and R9 the modes $k_{\parallel} = 0$ and $k_{\perp} = 0$ respectively are forced preferentially. In particular the amplitude of a Fourier mode $\mathbf{F}_{\mathbf{k}}$ of the forcing inside the chosen spherical shell was proportional to:

$$\text{R8: } |\mathbf{F}_{\mathbf{k}}| \propto \frac{k_x^2 + k_y^2}{k^2}, \quad \text{R9: } |\mathbf{F}_{\mathbf{k}}| \propto \frac{k_z^2}{k^2}, \quad (4)$$

where $k^2 = k_x^2 + k_y^2 + k_z^2$. Thus in run R8 the 2D modes ($k_z = 0$) are forced preferentially while in run R9 these

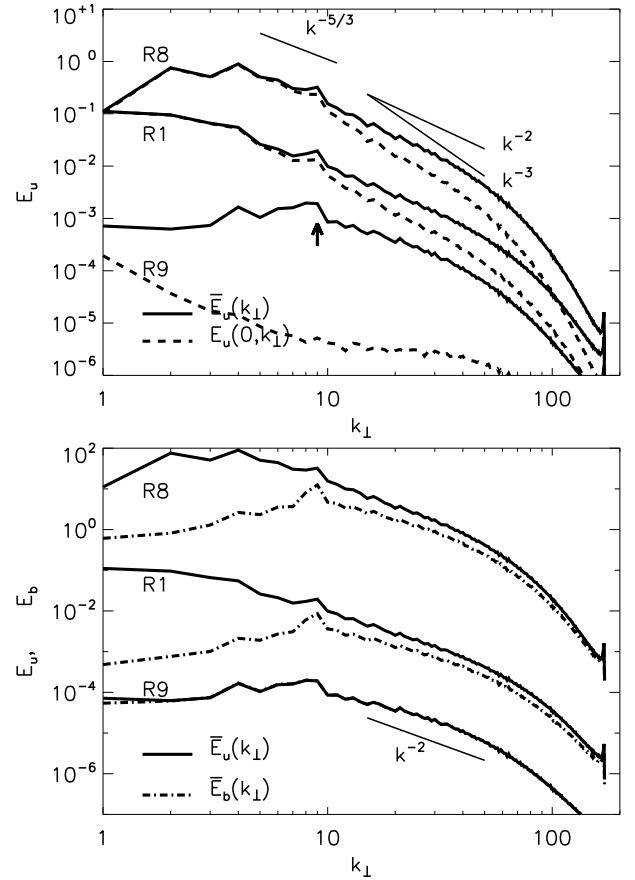


FIG. 12. Top panel: The kinetic energy spectra of $\bar{E}_u(k_{\perp})$ (solid line), and $E_u(0, k_{\perp})$ (dashed line) for R8, (top lines), R1, (middle lines), R9 (bottom lines) Bottom panel: The kinetic energy spectra $E_u(k_{\perp})$ (solid line), compared to the magnetic energy spectra $\bar{E}_b(k_{\perp})$ (dashed line) of the same runs and with the same order. The spectra have been shifted for reasons of clarity.

2D modes are not forced at all and most forcing is at the high k_z modes.

The energy flux for these runs is shown in figure 11. The energy flux of run R1 and R8 are very close for both directions. The reason for the slightly smaller flux of R8 at the largest scales is because R8 was evolved for a shorter time than R1. R9 however has no inverse cascade in the perpendicular direction (top panel). This is not surprising since for this run the 2D modes are not forced at all. In the parallel direction there is also a drastic change. R9 shows an inverse cascade from the large k_z wavenumbers to the 2D $k_z = 0$ modes. It is noted that the flux towards the large parallel scales was strongly fluctuating taking both positive and negative values. Only after averaging several files the result shown in figure 11 was obtained.

The spectra for these runs are shown in figure 12. Again not a lot of difference can be seen between run R1 and R8. Both are close to two-dimensional in the large scales and three dimensional in the small scales (top

panel), and both have weak magnetic energy in the large scales but are close to equipartition in the small scales (bottom panel). R9 on the other hand is three dimensional for all scales and kinetic and magnetic energy are almost identically equal at all scales. This last remark indicates that Alfvén-waves (for which $\mathbf{u} = \pm \mathbf{b}$) dominate the turbulence.

IV. SUMMARY AND DISCUSSION

In this work we have shown that under certain conditions an MHD-flow in the presence of a strong magnetic field can behave like a two dimensional flow in the large scales while like three dimensional (possibly weak turbulence) in the small scales, much like strongly rotating fluids. In the large scales it was found that the magnetic fluctuations were suppressed and a 2D inverse cascade of energy developed with energy accumulating in the large scales.

This inverse cascade however is sensitive to various parameters. If the uniform magnetic field amplitude is decreased sufficiently, or if the domain size is increased (or equivalently the forcing scale is decreased) so that the condition (2) for two-dimensionalization no longer holds the flow recovers its 3D behavior and cascades the energy forward. Furthermore, in the case that an electro-motive force is introduced although the flow remains 2D in the large-scales the magnetic fluctuations are no longer suppressed and the flow behaves like a 2D-MHD fluid with a direct energy cascade. At the same time an indication of an inverse cascade of the squared vector potential was observed. Finally, absence of an inverse cascade in the perpendicular direction was also observed when the system was forced only in the large k_{\parallel} modes. In this case an inverse cascade in the direction parallel to the magnetic field was observed.

All the simulations presented here that exhibited an inverse cascade, were stopped before the largest scale of

the system was reached due the computational cost. If the runs were continued for a longer time as the energy and the perpendicular wave number are increased it is possible that a point will be reached that the strength of the magnetic field will not be sufficient to stop three dimensional instabilities from breaking the two dimensional constrain. Such a transition point is expected to appear when the eddy turn over frequency $u_k k_{\perp}$ becomes smaller than the Alfvén frequency $B_0 k_{\parallel}$. In the inertia range of the inverse 2D cascade where the $k_{\perp}^{-5/3}$ scaling is expected the eddy turn over frequency is decreasing as larger scales are reached. On the contrary the smallest Alfvén frequency $B_0 k_{\parallel}$ remains independent of k_{\perp} . Thus the ratio $u_k k_{\perp}/B_0 k_{\parallel}$ will decrease as the cascade proceeds and it is not expected that such a transition point will exist in the inertial range, instead as the cascade proceeds the flow will come closer to a 2D flow. However since there is no large-scale damping mechanism to dissipate the energy when the largest scale of the system is reached the energy would pile up in this scale. In this case the eddy turn over frequency will increase and eventually the criterion (2) for two-dimensionality will be violated. Then energy could possibly return to the small scales as weak or strong turbulence. Similar scenario for the fate of the inverse cascade of rotating turbulence has been proposed in [32]. Such scenarios however need to be verified by numerical simulations and experiments.

ACKNOWLEDGMENTS

Computations were carried out on the CEMAG computing center on the CINES computing center, and their support is greatly acknowledged. The author would also like to thank the participants of the participants of the “Dynamics and turbulent transport in plasmas and conducting fluids” workshop in Les Houches, France March 2011 for their useful discussions and suggestions.

-
- [1] Ya. B. Zeldovich, A. A. Ruzmaikin, and A. A. Sokoloff, *Magnetic Fields in Astrophysics* (Gordon and Breach, 1990).
 - [2] S. Galtier, S. V. Nazarenko, A. C. Newell, and A. Pouquet, “A weak turbulence theory for incompressible magnetohydrodynamics,” *J. Plasma Phys.* **13**, 447–488 (2000).
 - [3] S. V. Nazarenko, *Wave Turbulence* (Springer-Verlag, 2011).
 - [4] S. V. Nazarenko, “2d enslaving of mhd turbulence,” *New J. Phys.* **9**, 307 (2007).
 - [5] D. Montgomery and L. Turner, “Anisotropic magnetohydrodynamic turbulence in a strong external magnetic field,” *Phys. Fluids* **24**, 825 (1981).
 - [6] Cho J. and E. T. Vishniac, “The anisotropy of magnetohydrodynamic alfvénic turbulence,” *Astrophys. J.* **539**, 273 (2000).
 - [7] J. Maron and P. Goldreich, “Simulations of incompressible magnetohydrodynamic turbulence,” *Astrophys. J.* **554**, 1175 (2001).
 - [8] J. Mason, F. Cattaneo, and S. Boldyrev, “Numerical measurements of the spectrum in magnetohydrodynamic turbulence,” *Phys. Rev. E* **77**, 036403 (2008).
 - [9] Beresnyak A. and Lazarian A., “Comparison of spectral slopes of magnetohydrodynamic and hydrodynamic turbulence and measurements of alignment effects,” *Astrophys. J.* **702**, 1190 (2000).
 - [10] A. Beresnyak, “Spectral slope and kolmogorov constant of mhd turbulence,” *Phys. Rev. Lett.* **106**, 075001 (2010).
 - [11] J. C. Perez and S. Boldyrev, “On weak and strong magnetohydrodynamic turbulence,” *Astrophys. J.* **672**, L61 (2007).
 - [12] B. Bigot, S. Galtier, and H. Politano, “Energy decay laws in strongly anisotropic magnetohydrodynamic tur-

- bulence,” *Phys. Rev. Lett.* **100**, 074502 (2008).
- [13] B. Bigot and S. Galtier, “Two-dimensional state in driven magnetohydrodynamic turbulence,” *Phys. Rev. E* **83**, 026405 (2011).
 - [14] R. H. Kraichnan, “Inertial ranges in two-dimensional turbulence,” *Phys. Fluids* **10**, 1417 (1967).
 - [15] C. E. Leith, “Diffusion approximation for twodimensional turbulence,” *Phys. Fluids* **11**, 671 (1968).
 - [16] G. K. Batchelor, “Computation of the energy spectrum in homogeneous twodimensional turbulence,” *Phys. Fluids* **12**, 233 (1969).
 - [17] L. Jacquin, O. Leuchter, C. Cambon, and J. Mathieu, “Structure and decay of rotating homogeneous turbulence,” *J. Fluid Mech.* **637**, 134–140 (2010).
 - [18] C. N. Baroud, B. B. Plapp, H. L. Swinney, , and Z.-S. She, “Scaling in three-dimensional and quasi-two-dimensional rotating turbulent flows,” *Phys. Fluids* **15**, 2091 (2003).
 - [19] P. D. Mininni and A. Pouquet, “Helicity cascades in rotating turbulence,” *Phys. Fluids* **79**, 026304 (2009).
 - [20] P. D. Mininni and A. Pouquet, “Rotating helical turbulence. i. global evolution and spectral behavior,” *Phys. Fluids* **22**, 035105 (2010).
 - [21] M. Thiele and W. Müller, “Structure and decay of rotating homogeneous turbulence,” *J. Fluid Mech.* **637**, 134–140 (2010).
 - [22] Antonio Celani, S. Musacchio, and D. Vincenzi, “Turbulence in more than two and less than three dimensions,” *Phys. Rev. Lett.* **104**, 184506 (2010).
 - [23] D. Fyfe and D. Montgomery, “High-beta turbulence in two-dimensional magnetohydrodynamics,” *J. Plasma Phys.* **16**, 181 (1976).
 - [24] A. Pouquet, “On two-dimensional magnetohydrodynamic turbulence,” *J. Fluid Mech.* **88**, 1 (1978).
 - [25] J. Sommeria, “Experimental study of the two-dimensional inverse energy cascade in a square box,” *J. Fluid Mech.* **170**, 138–168 (1986).
 - [26] P. Tabeling, B. Perrin, and S. Fauve, “Instability of a linear array of forced vortices,” *Europhys. Lett.* **3**, 459 (1987).
 - [27] D. O. Gomez, P. D. Mininni, and P. Dmitruk, *Adv. Space Res.* **35**, 899 (2005).
 - [28] D. O. Gomez, P. D. Mininni, and P. Dmitruk, *Phys. Scr. T* **116**, 123 (2005).
 - [29] A. Alexakis, B. Bigot, Politano H., and S. Galtier, “Anisotropic fluxes and nonlocal interactions in magnetohydrodynamic turbulence,” *Phys. Rev. E* **76**, 056313 (2007).
 - [30] S. Servidio and V. Carbone, “Nonlinear dynamics of inviscid reduced mhd plasmas: the appearance of quasi-single-helicity states,” *Phys. Rev. Lett.* **95**, 045001 (2005).
 - [31] P. Dmitruk, P. D. Mininni, A. Pouquet, S. Servidio, and W. H. Matthaeus, “Emergence of very long time fluctuations and $1/f$ noise in ideal flows,” *Phys. Rev. E* **83**, 066318 (2011).
 - [32] Sergei V. Nazarenko and Alexander A. Schekochihin, “Critical balance in magnetohydrodynamic, rotating and stratified turbulence: towards a universal scaling conjecture,” *J. Fluid Mech.* **677**, 134–153 (2011).